Placed on: Osaka City University Repository

Journal of Geosciences, Osaka City University
Vol. 28, Art. 4, p. 105-123
March, 1985

Strain and Size Analyses from X-ray Line Broadening of Pulverized Quartz

Hiroyuki NAGAO and Nobuyuki AIKAWA

(With 5 Figures, 5 Tables and 1 Plate)

Abstract

Described is an original procedure analysing a breadth of a broadened X-ray line profile by a pattern fitting technique to evaluate microstrain and crystallite size of pulverized quartz. This procedure is enough satisfactory for either a mean crystallite size of less than 200 nm or mean microstrain of greater than 2×10^{-4}. Natural quartz minerals have a wide variety in microstrain and crystallite size.

1. Introduction

Corresponding to their own histories all natural crystals must possess structural imperfections, such as grain boundaries, dislocations and impurities, most of which enlarge the free energy. An embodyment of this idea seems to be a broadened X-ray diffraction line profile, a main topic in this paper.

This subject has a considerable history, reaching back to the 1920's (VAN ARKEL, 1925). Broadening of an X-ray diffraction profile arises both from lattice parameter variations due to lattice microstrains or fluctuations in the chemical composition and from small sizes of X-ray coherent domains. The informations about them should be given by the X-ray line broadening analysis although they were not always of satisfying quality. Extraordinary many contributions have been published especially for experimentally deformed metal crystals (see KLUG and ALEXANDER, 1954; GUINIER, 1956; TAYLOR, 1961).

X-ray line broadening studies on minerals, either of experimentally deformed materials or of natural virgin ones, have been restricted to calcite, quartz and some few minerals chiefly because the fluctuation in the chemical composition interferes with the quantitative analysis of a line profile. ROSENTAHL and KAUFMANN (1952) examined experimentally deformed calcite powders of various diameters, in which residual strains relaxed by pulverization was predominant. PATERSON (1959) and GROSS (1965) also studied experimentally deformed calcites to show that they had larger stored energy, calculated from the internal microstrain, than metal crystals and gave kinetic coefficients for static recovery and recrystallization of calcite. In the 1970's X-ray line broadening studies were applied to experimentally shock-loaded products. Some authors demonstrated a gradual deformatoin of quartz, a decrease in the mean crystallite size and an increase in

internal microstrains, with shock pressure (HÖRTZ and QUAIDE, 1973; HANSS *et al.*, 1978; SCHNEIDER *et al.*, 1984).

X-ray line broadening has also described the wide variety in natural minerals from different occurrences. GROSS and PATERSON (1965) demonstrated that some natural calcite showed significant line broadening and ascribed it to lattice microstrains. Quartz from metachert in a low P/T type regional metamorphic belt show also significant line broadening attributed to internal microstrains (NAGAO and AIKAWA; 1983). They tried to make use of the broadening as an indicator of past geologic deformation. As concerns poorly crystallized materials, quartzose cherts recovered from deep-sea sediments shows the wide range in line broadening (HATHAWAY, 1972). MURATA and NORMAN (1976) proposed a crystallinity index (C.I.) for quartz based on the degree of resolution of the 212 doublet, the broadening of which was ascribed mainly to small coherent domains. The cause of X-ray line broadening does not seem to be so simple because some chalcedonic quartz in zoned agates obviously shows both strain broadening and size broadening, whereas other shows size braodening only (FLORKE *et al.*, 1982; MIEH *et al.*, 1984).

X-ray line broadening analysis has the advantage that the magnitude of microstrain is readily assessed and the volume mean value of many grains from a specimen is easily available. These merits must be useful for geologic purposes in that microstrains and/or crystallite sizes may result from, or in, the solid state reaction kinetics of geologic phenomena.

The use of the line breadth as an indicator for the X-ray line broadening is so convienient and speedy that it seems to the present authors enough satisfactory for geological researches as long as its limitations are generally realized. This paper describes an original procedure analysing a breadth of a broadened X-ray line profile of pulverized quartz by a pattern fitting technique to distinguish between the broadening due to microstrain and the broadening due to crystallite sizes with discussion about the limitation of a line breadth analysis. Some quartz minerals were preliminarily examined, the results are also presented. In this paper the terms of "microstrain" and "crystallite size" are to be used as a degree of non-uniform displacements of the interplanar spacing of the crystal lattice from its mean value and a linear dimension perpendicular to the reflecting planes within which the crystal is coherent in X-ray diffraction, respectively.

2. Preparation of specimens and X-ray diffractometry

The studied samples are briefly explained in Appendix 2. The samples were crushed into powders with a range of diameters from 63 μm to 125 μm. If necessary, the powders were purified in hot phosphoric acid for an hour or two until no impurity except quartz remained detectable by X-ray powder diffractometry. There was no practical change in X-ray line profiles during the chemical treatment. The powders were then ground by an automatic agate-mortar for ten minutes and limited from 5 μm to 20 μm, obtanied by means of sieving with 20 μm meshes and precipitation in ethanol using the Stokes'

formula. Although little or no plastic deformation occurs during the grinding process judging from the observation by BURSILL and MCLAREN (1965), very fine particles made during the grinding may effect X-ray line profiles. The scanning electron microscope (SEM) observation showed that the grinding for ten minutes made little amounts of powders of less than 1μm in diameter and most of them were removed by the precipitation procedure. In practice the grinding for more than an hour made a line profile a little broadened, however, this was not the case for the grinding for less than half an hour. For X-ray analysis the powdered quartz was carefully mounted on a glass-holder with a space of $16\times 20\times 0.2$ mm for powder specimens.

The powder diffractometer RIGAKU RAD-1A was used in this study. Diffraction profiles of hh0 reflections, namely 110, 220 and 330 reflections, were obtained by the $\omega-2\theta$ step scanning technique. If a specimen gave so severe line broadening that the 330 reflection was not detectable, the analyses were performed with 110 and 220 reflections only. The experimental conditions were as follows: radiation, copper K_α with nickel filter, 45 KV 25 mA; take-off angle from X-ray tube target, approximately 6°; incident beam divergence, 1°; receiving slit, 0.15 mm; scatter slit, 1°; scanning step, 0.002° or 0.004° (2θ). Other experimental conditions are tabulated in Table 1. The reasons why the hh0 reflections were adopted are that a set of three reflections from parallel reflecting planes are available using the copper K_α radiation and that they are expected to be the most broadened reflections by dislocation slip because the basal slip system, the easiest dislocation slip system of low quartz at ordinary geologic temperatures, is (001)$\langle$110$\rangle$.

3. Profile breadth analysis

After the original intensity data were slightly smoothed by five or eleven neighbouring points, the background was eliminated. Calculated line profiles, presumed to be a symmetric Modified-Lorentzian function in shape, were to be fitted to the observed intensity profile changing parameters of the calculated line profiles in turn to search the parameters of the best fitted profile. The rationality for this presumption is to be referred to the Appendix 1. Assuming that the profiles due to $K_{\alpha 1}$ and $K_{\alpha 2}$ radiations are of the same shape and additive except that the former is just twice the intensity of the latter, thus, the total intensity $I(\theta)$ is given by

$$I(\theta)=I_0(1+w(\theta-\theta_0)^2)^{-2}+\frac{I_0}{2}(1+w(\theta-\theta_0-\Delta\theta)^2)^{-2} \qquad (1)$$

where the first term and the second term are the intensity components of $K_{\alpha 1}$ and $K_{\alpha 2}$ radiations, respectively, I_0 is the maximum intensity of the line profile for the $K_{\alpha 1}$ radiation, θ_0 is its peak position, w is a parameter for the line breadth and $\Delta\theta$ is an angular interval between peak positions of the K_α doublet which depends on θ_0 only (Fig. 1).

The parameter for a line breadth, w, is related to the full breadth at half maximum,

Table 1. Experimental conditions of X-ray diffractometry and results of the profile fitting analyses. Peak angle, Max. intensity, Int. intensity, H.M. breadth and Integral breadth are those of a line profile due to $K_{\alpha 1}$ radiation. All values related with the diffraction angle are expressed in 2 values, Max. intensity: maximum intensity, Int. intensity: integrated intensity, H.M. breadth: half maximum breadth.

Sample name	IK 01			KA 01			KA 01b			KA 02			KA 03		
Profile index	110	220	330	110	220	330	110	220	330	110	220	330	110	220	330
Scanning from (°)	35.8	77.0	139.5	35.5	76.5	139.5	35.5	76.5	139.5	35.8	76.5	139.5	35.8	76.5	139.5
Scanning to (°)	37.3	78.5	142.0	37.5	78.5	142.0	37.5	78.5	142.0	37.3	78.5	142.0	37.3	78.5	142.0
Scanning step (°)	.002	.002	.004	.004	.004	.004	.004	.004	.004	.002	.002	.002	.002	.002	.002
Smoothing points	5	5	5	5	11	11	5	11	11	5	11	11	5	11	11
Peak angle (°)	36.518	77.648	140.346	36.478	77.614	140.292	36.483	77.618	140.316	36.530	77.668	140.384	36.491	77.624	140.324
Max. intensity (°)	4818	782.5	494.6	22580	3227	635.4	9668	1351	276.3	8656	1196	577.8	7750	1075	484.2
Back ground (ct)	142.4	131.7	337.8	934.3	791.0	972.2	1439	959.8	1048	348.4	291.0	919.0	479.1	379.8	1129
Int. intensity(°ct)	587.0	116.6	146.1	3288	605.4	297.8	2024	345.8	160.3	1286	240.8	313.0	1176	226.0	269.8
H.M. breadth (°)	.0930	.1180	.2240	.1150	.1520	.3780	.1550	.1870	.4260	.1190	.1640	.4380	.1230	.1700	.4580
Int. breadth (°)	.1218	.1491	.2953	.1456	.1876	.4687	.2094	.2559	.5804	.1486	.2014	.5417	.1518	.2103	.5572
R_f (%)	3.96	1.88	3.72	2.09	0.767	3.63	3.83	2.89	11.0	2.24	0.850	3.14	2.13	0.901	3.62

Sample name	KA 04			KA 05			OT 01			OT 02			OT 03		
Profile ndex	110	220	330	110	220	330	110	220	330	110	220	330	110	220	330
Scanning from ( )	35.8	77.0	139.5	35.8	77.0	139.5	35.8	77.3	139.7	35.8	76.5	139.5	35.8	76.5	139.5
Scanning to (°)	37.3	78.5	142.0	37.3	78.5	142.0	36.8	78.2	140.8	37.3	78.5	142.0	37.3	78.5	142.0
Scanning step (°)	.002	.002	.002	.002	.0042	.002	.002	.002	.004	.002	.002	.002	.002	.002	.002
Smoothing points	5	11	11	5	11	11	5	11	11	5	11	11	5	11	11
Peak angle (°)	36.507	77.642	140.342	36.474	77.622	140.332	36.501	77.634	140.324	36.508	77.630	140.284	36.517	77.634	140.270
Max. intensity (ct)	8296	1529	878.0	8843	1616	1122	8558	1280	675.9	8415	1270	641.2	7677	2634	489.1
Back ground (ct)	292.7	241.3	823.8	299.8	244.2	828.1	274.9	259.5	813.6	257.3	230.7	781.5	585.9	1224	1386
Int. intensity(°ct)	1238	261.0	335.0	1244	261.3	370.6	1193	223.3	188.4	1221	255.6	333.0	1125	550.5	254.4
H.M. breadty (°)	.1190	.1350	.2980	.1130	.1270	.2520	.1140	.1430	.3240	.1160	.1600	.4220	.1170	.1700	.4360
Int. breadth (°)	.1492	.1706	.3816	.1407	.1617	.3303	.1394	.1744	.4181	.1451	.2012	.5193	.1466	.2090	.5200
R_f (%)	2.22	1.53	2.64	2.80	1.84	3.11	2.57	1.43	9.73	2.27	1.060	3.12	2.14	0.867	3.05

Sample name	OT 04			OT 05			ON 01			UN 01		UN 02	
Profile index	110	220	330	110	220	330	110	220	330	110	220	110	220
Scanning from (°)	35.8	76.5	139.5	35.6	76.5	139.0	35.8	77.0	139.5	35.8	76.5	35.8	76.5
Scanning to (°)	37.3	78.5	142.0	37.5	78.5	142.0	37.3	78.5	142.0	37.3	78.5	37.3	78.5
Scanning step (°)	.002	.002	.002	.002	.004	.004	.002	.002	.002	.002	.002	.002	.002
Smoothing points	5	11	11	5	11	11	5	11	11	5	11	5	11
Peak angle (°)	36.507	77.622	140.226	36.503	77.634	140.308	36.504	77.642	140.354	36.508	77.606	36.510	77.616
Max. intensity (ct)	7940	3008	544.6	8704	1178	214.6	8644	1233	646.2	3940	1316	3618	1135
Back ground (ct)	497.3	976.7	1171	412.5	327.0	423.1	375.1	300.5	975.6	937.4	1663	464.6	952.8
Int. intensity(°ct)	1165	615.4	273.2	1285	247.8	100.8	1277	251.3	310.9	901.7	461.8	1061	491.2
H.M. breadth (°)	.1140	.1580	.4120	.1170	.1670	.3860	.1180	.1630	.3980	.1820	.2780	.2350	.3580
Int. breadth (°)	.1467	.2046	.5017	.1476	.2104	.4696	.1478	.2039	.4812	.2289	.3508	.2932	.4327
R_f (%)	2.60	1.40	2.81	2.21	1.27	2.87	2.62	1.52	2.44	2.40	2.35	2.69	2.20

Sample name	AG 01		AG 02		AG 03		AG 04		
Profile index	110	220	110	220	110	220	110	220	330
Scanning from (°)	35.8	76.5	35.8	76.5	35.8	76.5	35.8	76.5	139.5
Scanning to (°)	37.3	78.5	37.3	78.5	37.3	78.5	37.3	78.5	142.0
Scanning step (°)	.002	.002	.002	.004	.002	.002	.002	.002	.002
Smoothing points	5	11	5	11	5	11	5	11	11
Peak angle (°)	36.515	77.602	36.500	77.594	36.485	77.600	36.517	77.638	140.294
Max. intensity (ct)	2243	642.3	2115	621.6	2811	896.0	9056	3078	1197
Back ground (ct)	462.1	866.1	464.2	872.2	434.0	830.8	266.4	621.3	804.4
Int. intensity(°ct)	779.7	351.8	782.3	366.6	822.4	380.4	1233	471.3	317.2
H.M. breadth (°)	.2830	.4670	.3080	.5020	.2370	.3430	.1080	.1210	.2000
Int. breadth (°)	.3476	.5478	.3698	.5898	.2926	.4246	.1362	.1531	.2649
R_f (%)	1.86	3.24	1.92	3.82	5.46	6.55	3.73	1.61	3.16

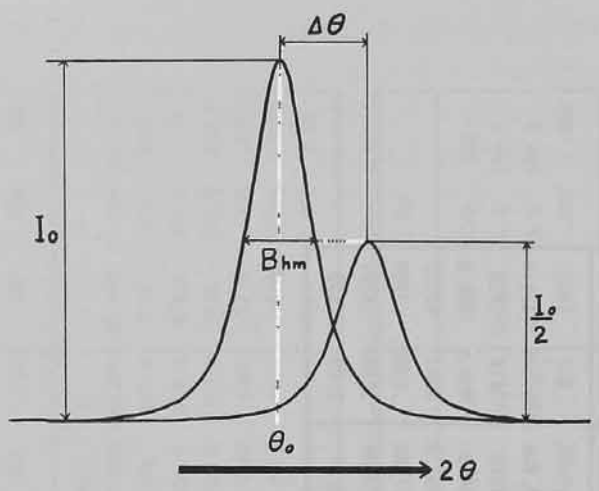

Fig. 1. Schematic line profile of K_α doublet with parameters used in text.

B_{hm}, defined as the angular breadth between the points where the intensity falls to half its maximum intensity value. From this definition, derived is the equation,

$$w = 4(\sqrt{2}-1)/B_{hm}^2 \qquad (2)$$

From equations (1) and (2),

$$I(\theta) = I_0(1+1.657(\theta-\theta_0)^2/B_{hm}^2)^{-2}+\frac{I_0}{2}(1+1.657(\theta-\theta_0-\Delta\theta)^2/B_{hm}^2)^{-2} \qquad (3)$$

For simplification, only B_{hm} and θ_0 in equation (3) were independently changed in the profile fitting program whereas I_0 was constrained to the value computed from the observed data. On giving B_{hm} and θ_0, uniquely led is the ratio of the intensity component due to $K_{\alpha 2}$ radiation to that due to $K_{\alpha 1}$ radiation at $\theta=\theta_0$ by the equation (4),

$$I_{K\alpha 2}(\theta_0)/I_{K\alpha 1}(\theta_0) = \frac{1}{2}(1+w(\Delta\theta)^2)^{-2} \qquad (4)$$

This allots the observed intensity at $\theta=\theta_0$ into two intensity components, which gives I_0 as its $K_{\alpha 1}$ part.

The profile fitting was performed minimizing the residuals, R_f, given by

$$R_f = (\sum(I(\theta)_{obs}-I(\theta)_{calc})^2)^{0.5}/I_0 \qquad (5)$$

The final step intervals were 0.001° or 0.002° (2θ) for both θ_0 and B_{hm}. In this study there was always one reasonable residual minimum for each profile fitting procedure. An integral breadth, B_i, the breadth of an ideal line which has uniform intensity equal to the maximum and an integrated intensity equal to that of the actual line, say,

$$B_i = \int I_{K\alpha 1}(\theta)d\theta/I_0 \qquad (6)$$

the integrations being carried out using the Simpson's rule. The results of the profile fitting procedure are listed in Table 1.

4. Correction for instrumental broadening

In order to obtain a breadth for *pure broadening* of a specimen, the broadening due to the experimental conditions (to be called as *instrumental broadening*) has to be eliminated. The instrumental broadening, consisting mainly of spectral broadening and broadening due to instrumental factors, was often assumed to be specimen independent and constant. The instrumental profile, however, should be recorded from a standard specimen, giving negligible broadening in itself, of the same composition that is treated in the same way, as far as possible, as the specimen under investigation (DE KEIJSER and MITTEMEIJER, 1977). It was obtained from a euhedral, colorless, transparent Brazillian rock crystal, from which powder specimens were prepared in the same procedure described in the chapter 2. The data for instrumental broadening are tabulated in Table 2.

Table 2. Adopted values of the integral breadths for instrumental broadening. Mean values of ten measurements.

Index	Instrumental breadth (deg.)
110	0.1211 ±0.004
220	0.1437 ±0.005
330	0.2635 ±0.009

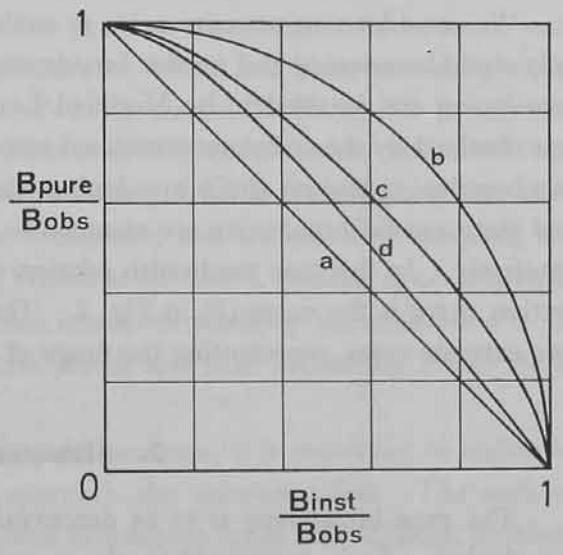

Fig. 2. Curves correcting line breadths for instrumental broadening with vairous kinds of presumptive profile shape functions.

It is necessary to presume profile shape functions for both pure broadening and instrumental broadening in order to obtain an increment relation of line breadths when two profiles are synthesized by convolution. For instance if both profile shapes are Lorentzian, $(1+wx^2)^{-1}$, or Gaussian, $\exp(-wx^2)$, then their breadths or the squares of their breadths are additive, respectively (WOOD and RACHINGER, 1949; WARREN, 1941). The schematic relations in these two cases are shown in Fig. 2, where (a) and (b) correspond to a profile shape of Lorentzian and that of Gaussian. It is noteworthy that these two curves are rather different, say, the correction is dependent on presumptive profile shape functions.

The profile shape analyses (Appendix 1) revealed the well similarity of the profile shape of instrumental broadening to Modified Lorentzian function, $(1+wx^2)^{-2}$. Modified Lorentzian function is, to the first approximation, of an intermediate curvature between Gaussian and Lorentzian functions.

On the other hand a profile shape for pure broadening depends on two broadening factors, lattice microstrains and small sizes of X-ray coherent domains. The broadened line profile due to lattice microstrains seemed to be well expressed by Gaussian or Modified Lorentzian functions whereas that due to size effects by Lorentzian function (cf. TAYLOR, 1961, p 789). The profile shape function for pure broadening should be variable according to the relative breadths of these two contributions.

The profile shape analyses of some kinds of samples tabulated in Appendix 1 have consistency with the assumption that strain broadening gives a Modified Lorentzian profile, rather than a Gaussian profile, and that size broadening gives a Lorentaizan profile. An actual profile shape function for pure broadening synthesized from two types of broadening is considered to be an intermediate nature between Modified Lorentzian and Lorentzian functions.

We consider two extreme cases to evaluate the pure broadening. First if there is only strain broadening and no size broadening, line profile for both instrumental and pure broadening are assumed to be Modified Lorentzian. The correction curve of this case was obtained by the computer-simulated convolution (Fig. 2-(c)). Second if there is only size broadening and no strain broadening, the profile shape function for pure broadening and instrumental broadening are assumed to be Lorentzian and Modified Lorentzian, respectively. In this case the beadth relation was given by SCHÖENING (1962) and the correction curve is the curve (d) in Fig. 2. The following analyses are to be done for both two extreme cases, representing the range of a true solution.

5. Size-strain analisis

The pure broadening is to be deconvoulted into the strain broadening and the size broadening. As is mentioned in the preceding chapter, the strain broadening and the size broadening is assumed to be expressed by Modified Lorentzian function and Lorentzian function, respectively. In this case the relation among three breadths, namely the breadth for strain broadening (B_{strain}), the breadth for size broadening (B_{size}) and the breadth for pure broadening into which the two types of broadening are synthesized (B_{pure}), is uniquely given by

$$B_{\text{pure}} = (2B_{\text{strain}}+B_{\text{size}})^2/(4B_{\text{strain}}+B_{\text{size}}) \qquad (7)$$

where B_{strain}, B_{size} and B_{pure} are the integral breadths (the half maximum breadths also will do) for three types of broadening (SCHÖENING; 1962).

As are shown in many literatures, strain broadening and size broadening are expressed by the equations

$$B_{\text{strain}} = 4\varepsilon \tan\theta \qquad (8)$$

$$B_{\text{size}} = K\lambda/D\cos\theta \qquad (9)$$

where ε is mean lattice microstrain, D is a mean crystallite size, λ is X-ray wavelength, K is a constant of near unity and θ is Bragg angle.

Using the equations (7)–(9), three (or two in some specimens) equations corresponding to three (or two) reflections are led where only two parameters, ε and D, are variable. As the reflections used are derived from parallel reflecting lattice planes, the values of ε and D should be common to all equations. They were valuated by a laest squares method, minimizing total residuals between the observed B_{pure} and calculated B_{pure} that are given under a certain ε and D, both of which were constrained to be positive. The analytical results are tabulated in Table 3.

6. Discussion

The earlier X-ray line broadening studies were usually content to use only line breadths. Later the interesting feature of a line profile became second-order ones, such as profile shapes, peak displacements and asymmetries, which had been missed by working only with line breadths (WARREN, 1959). For this reason the X-ray line broadening analyses using Fourier series proposed by STOKES (1948) and WARREN and AVERBACH (1950, 1952) were usually adopted. In spite of some inevitable systematic errors, such as the uncorrected constant background, the truncation, and the effect of sampling the observed profile at a finite number of points (YOUNG *et al.*, 1967), because of no presumption about a profile shape function, the Fourier transform methods are considered to be very powerful for deducing the pure diffraction profile and then separating it into strain broadening and size broadening.

On the other hand, concerning the line breadth analyses, it is important to realize to what extent the line breadth analyses can approach the accurate value. The authors have believed that the correction for instrumental broadening is the most difficult problem in the line breadth analyses. It is because a profile shape function for pure broadening, on which the instrumental correction of a line breadth depends, is not fixed as is mentioned in chapter 4.

The relation among the three sorts of the breadths, the breadth of the observed profile, that of the instrumental profile and that of the pure profile, is essential to get the breadth of the pure profile from the other breadths experimentally obtained. Some of the breadth correction curves are shown in Fig. 4. They were determined by solving the integral equation called as convolution,

(1) using the presumptive profile shape functions of both pure and instrumental profiles (a,d,e).

(2) using the presumptive profile shape functions of both observed and instrumental profiles (c, f).

Table 3. Results of strain and crystallite size analysis. All values related with the diffraction angle are expressed in 2 values. Type (c) and (d): the cases that the correction curve (c) and (d) in Fig. 2 were adopted in the instrumental correction, respectively.

Sample name	IK 01		KA 01		KA 01b		KA 02		KA 03		KA 04		KA 05	
Type	(c)	(d)	(c)	(d)	(c)	(d)	(c)	(d)	(c)	(d)	(c)	(d)	(c)	(d)
Pure (110)	.0080	.0009	.0511	.0320	.1320	.1109	.0554	.0358	.0599	.0399	.0563	.0366	.0437	.0257
breadth (220)	.0224	.0070	.0810	.0568	.1655	.1404	.0987	.0741	.1103	.0851	.0574	.0352	.0438	.0237
(°) (330)	.0782	.0419	.3028	.2568	.4324	.3878	.3882	.3429	.4060	.3609	.1972	.1511	.1303	.0869
Strain ($\times 10^{-4}$)	1.23	0.63	4.18	3.97	2.18	2.50	6.00	5.28	6.00	5.59	1.55	1.66	0.62	0.67
Size (nm)	–	–	–	560	75	94	–	–	860	–	220	480	250	500
R.M.S. (°)	.0008	.0036	.0078	.0099	.0039	.0051	.0095	.0143	.0071	.0110	.0094	.0096	.0053	.0052

Sample name	OT 01		OT 02		OT 03		OT 04		OT 05		ON 01	
Type	(c)	(d)	(c)	(d)	(c)	(d)	(c)	(d)	(c)	(d)	(c)	(d)
Pure (110)	.0416	.0240	.0503	.0314	.0525	.0333	.0527	.0334	.0540	.0346	.0543	.0348
breadth (220)	.0630	.0401	.0984	.0739	.1087	.0835	.1030	.0781	.0224	.0070	.1021	.0772
(°) (330)	.2426	.1959	.3623	.3167	.3632	.3176	.3418	.2960	.0782	.0419	.3177	.2717
Strain ($\times 10^{-4}$)	3.36	3.01	5.51	4.90	5.17	4.96	4.68	4.62	1.23	0.63	3.93	4.20
Size (nm)	740	–	–	–	570	–	450	–	230	660	300	–
R.M.S. (°)	.0094	.0074	.0054	.0106	.0012	.0054	.0017	.0045	.0057	.0039	.0004	.0016

Sample name	UN 01		UN 02		AG 01		AG 02		AG 03		AG 04	
Type	(c)	(d)	(c)	(d)	(c)	(d)	(c)	(d)	(c)	(d)	(c)	(d)
Pure (110)	.1551	.1340	.2286	.2085	.2890	.2698	.3133	.2945	.2279	.2079	.0368	.0199
breadth (220)	.2745	.2507	.3650	.3427	.4893	.4686	.5341	.5139	.3562	.3337	.0308	.0124
(°) (330)												
Strain ($\times 10^{-4}$)	9.54	9.60	10.14	10.18	15.63	15.74	17.33	17.46	9.32	9.38	0.00	0.00
Size (nm)	91	120	51	59	45	50	42	47	50	57	790	–
R.M.S. (°)	.0004	.0005	.0003	.0005	.0003	.0005	.0003	.0004	.0003	.0004	.0195	.0115

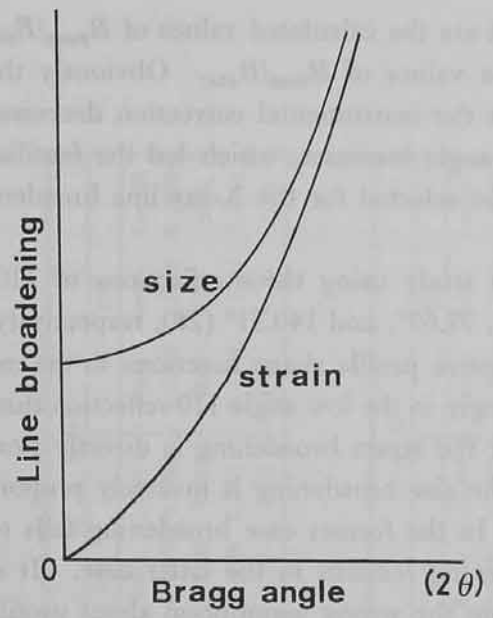

Fig. 3. Schematic angular dependence of line breadth caused by crystallite size effects and by microstrain effects.

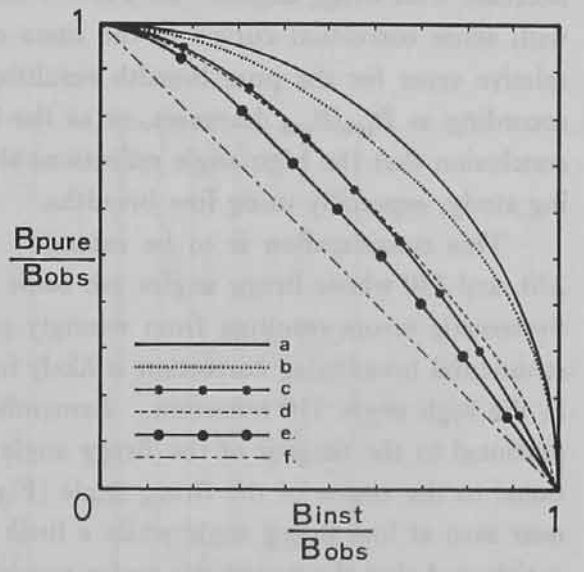

Fig. 4. Correction curves for the instrumental broadening. a: WARREN (1941), b: JONES (1938) Fig. 3(a), c: SCHÖENING *et al.* (1952), d: This paper Fig. 2(c), e: This paper Fig. 2(d), f: WOOD and RACHINGER (1949).

(3) using an experimentally determined instrumental profile and the presumptive profile shape function of a pure profile (b).

The correction curves are rather diverse from each other and may introduce the systematic error into the corrected line breadth.

The pure line breadth, irrespective cause of broadening (size or strain), increases rapidly with Bragg angle as is illustrated in Fig. 3. So, in general, the ratio of the B_{pure} B_{obs} has a tendency to increase with Bragg angle while the ratio of the $B_{\text{inst}}/B_{\text{obs}}$ tends to

Table 4. The model calculation of the instrumental broadening. The values of $B_{\text{pure}}/B_{\text{obs}}$ corresponding to some values of $B_{\text{puer}}/B_{\text{obs}}$ are calculated using for correction curves in Fig. 2 to demonstrate that the relative error (e) decreases according as $B_{\text{Inst}}/B_{\text{obs}}$ decreases.

Binst / Bobs	Bpure / Bobs (1)	(2)	(3)	(4)	(5)
0.90	0.44	0.25	0.13	0.10	4.40
0.60	0.80	0.61	0.50	0.40	2.00
0.30	0.95	0.87	0.82	0.70	1.36

(1) using correction curve (b) in Fig.2
(2) using correction curve (c) in Fig.2
(3) using correction curve (d) in Fig.2
(4) using correction curve (a) in Fig.2
(5) ratio of the value in (1) to the value in (4)

decrease with Bragg angles. In Table 4 tabulated are the calculated values of B_{pure}/B_{obs} with some correction curves in the cases of some values of B_{inst}/B_{obs}. Obviously the relative error for the pure breadth resulting from the instrumental correction decreases according as B_{int}/B_{obs} decreases, or as the Bragg angle increases, which led the familiar conclusion that the high angle reflections should be selected for the X-ray line broadening study, especially using line breadths.

This consideration is to be extended to this study using three reflections of 110, 220, and 330 whose Bragg angles are some 36.55°, 77.67°, and 140.31° (2θ), respectively. Systematic errors resulting from wrongly presumptive profile shape functions in the instrumental broadening correction is likely to be larger in the low angle 110 reflection than in the high angle 330 reflection. Remember that the strain broadening is directly proportional to the tangent of the Bragg angle and the size broadening is inversely proportional to the cosine of the Bragg angle (Fig. 3). In the former case broadening falls to near zero at low Bragg angle while a little broadening remains in the latter case. It is anticipated that the systematic errors resulting from the wrong assumption about profile shape functions, on the whole, are ascribed to the broadening due to size effects and that they hardly effect the value of microstrain.

The final results tabulated in Table 4 are ploted in Fig. 5. The tied points are the

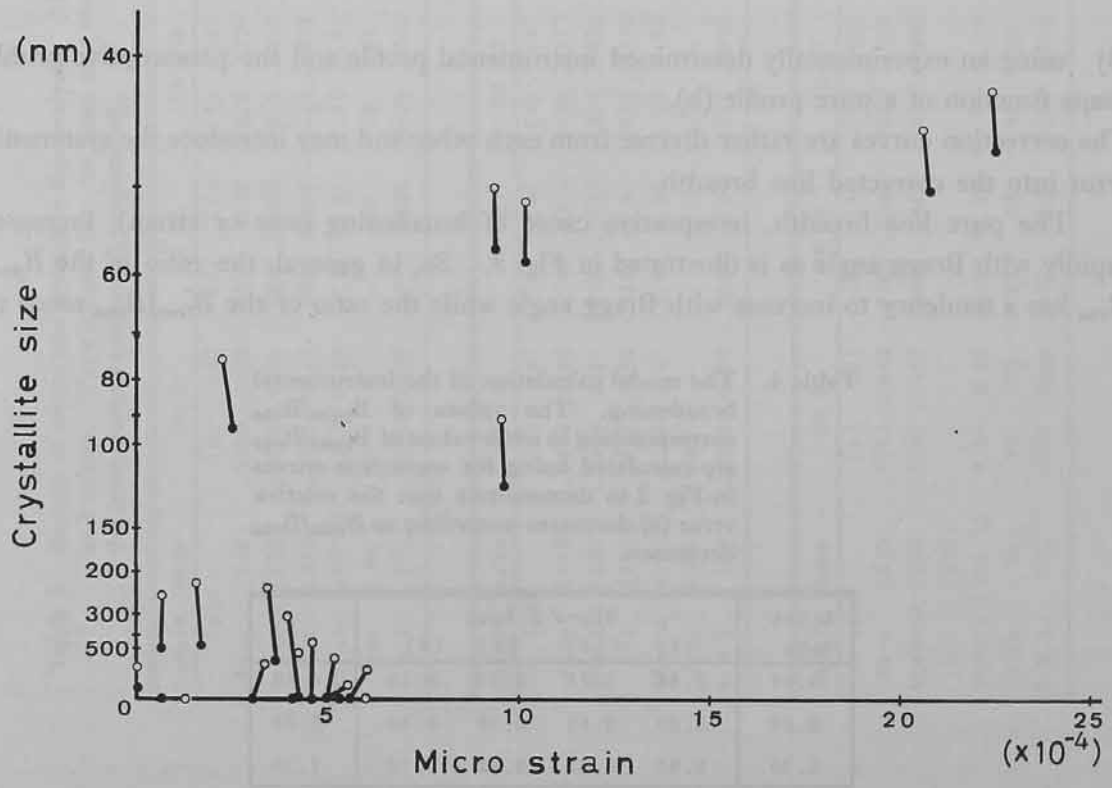

Fig. 5. Estimated values of microstrain and crystallite sizes. The scales of two axes are normallized by the equal degree of line broadening at 70° (2θ). The tied points are the data from the same specimen but the instrumental correction was performed using different correction curves.

Table 5 Results of profile shape function analysis. Gauss: Gaussian function, Mod-L: Modified Lorentzian function, Lorent: Lorentzian function. See also Table 1.

(a) Samples showing only instrumental broadening

Sample name	NST00						NST01					
Index	110			220			110			220		
Function	Gauss	Mod-L	Lorent	Gauss	Mod-L	Lorent	Gauss	Mod-L	Lorent	Gauss	Mod-L	Lorent
H.M.breadth (°)	0.0930	0.0880	0.0800	0.1170	0.1060	0.0950	0.1030	0.0970	0.0880	0.1150	0.1030	0.0900
Max. intensity	11230	11010	10950	1681	1670	1647	25660	25330	25270	5649	5701	5680
Int.breadth (°)	0.1108	0.1131	0.1137	0.1339	0.1348	0.1367	0.1213	0.1228	0.1231	0.1319	0.1307	0.1312
R_f (%)	4.01	3.17	3.64	2.23	1.03	2.04	4.46	3.62	4.19	2.87	1.79	2.10

(b) Samples showing large strain broadening and little size broadening

Sample name	KA 03						KA 02					
Index	110			220			110			220		
Function	Gauss	Mod-L	Lorent	Gauss	Mod-L	Lorent	Gauss	Mod-L	Lorent	Gauss	Mod-L	Lorent
H.M.breadth (°)	0.1370	0.1230	0.1090	0.1790	0.1700	0.1550	0.1320	0.1190	0.1060	0.1740	0.1640	0.1500
Max. intensity	7606	7750	7851	1103	1075	1059	8539	8656	8762	1224	1196	1172
Int.breadth (°)	0.1546	0.1518	0.1498	0.2050	0.2103	0.2135	0.1506	0.1486	0.1468	0.1968	0.2104	0.2055
R_f (%)	3.76	2.13	3.57	2.50	0.90	2.47	3.83	2.24	3.51	2.36	0.85	2.58

(c) Samples showing both strain broadening and size broadening

Sample name	OT 05						UN 12					
Index	110			220			110			220		
Function	Gauss	Mod-L	Lorent	Gauss	Mod-L	Lorent	Gauss	Mod-L	Lorent	Gauss	Mod-L	Lorent
H.M.breadth (°)	0.1290	0.1170	0.1050	0.1760	0.1670	0.1520	0.2060	0.1820	0.1580	0.3010	0.2780	0.2510
Max. intensity	8637	8704	8775	1207	1178	1155	3816	3940	4061	1328	1316	1318
Int.breadth (°)	0.1488	0.1476	0.1464	0.2053	0.2104	0.2145	0.2363	0.2289	0.2220	0.3476	0.3508	0.3503
R_f (%)	3.78	2.21	3.15	2.91	1.27	2.03	5.54	2.40	2.06	5.42	2.35	2.52

(d) Samples showing large size broadening and little strain broadening

Sample name	KA 01b					
Index	110			220		
Function	Gauss	Mod-L	Lorent	Gauss	Mod-L	Lorent
H.M.breadth (°)	0.1760	0.1550	0.1340	0.1940	0.1870	0.1730
Max. intensity	9293	9668	10040	1392	1351	1326
Int.breadth (°)	0.2178	0.2094	0.2016	0.2484	0.2559	0.2608
R_f (%)	5.70	3.83	3.18	4.53	3.89	2.26

values from breadth data of the same specimen, the open circle and the solid circle correspond to the cases that the corrections for instrumental broadening were performed using the correction curves (c) and (d) in Fig. 2, respectively,. It is demonstrated that the values of the crystallite size have a wide range as a result of the instrumental broadening correction, while corresponding microstrain values are well consistent. Considering that the inverse of the crystallite size contributes the line broadening while the strain is directly proportional to it, the absolute value of the crystallite size is strongly dependent on the presumptive profile shape function in the instrumental broadening correction.

The fact that the lengths of the tie-lines in Fig. 5 are roughly equal to each other implies that the relative errors resulting from the instrumental broadening correction do decrease according as the degree of line broadening incraeses. The line broadening analysis using line breadth is enough satisfactory for either a mean crystallite size of less than 200 nm or mean microstrain of greater than 2×10^{-4}. In practice the line breadth analysis is also a rather powerful tehcnique for studies about natural quartz, especially for its microstrain analysis. Fig. 5 also demonstrated that natural quartz minerals have a wide varieties in microstrain and crystallite sizes, which will be discussed in another paper.

Acknowlegement

The calculation was assisted by Mr. S. MASUMOTO to whom the authors are indebted.

Appendix 1. Profile shape analysis

In recent profile shape analyses introduced are several profile shape functions, most of which are derived from two principle functions: Gaussian function, $\exp(-wx^2)$, and Lorentzian function, $(1+wx^2)^{-1}$ (*cf.* YOUNG and WILES, 1928). Modified Lorentzian function, $(1+wx^2)^{-2}$, is often used as a variety of Lorentzian function. Profile shape function analyses on observed X-ray line profiles of some kinds of specimens were performed.

The analyses were done by comparison with the root-mean-square residuals, R_f, changing the calculated profile shape functions in the profile fitting procedure. The influence of the presumptive profile shape function on the value of the integral breadth is also examined. The profiles of only 110 and 220 were examined because some of the 330 profiles were too severely broadened to analyse profiles. The results are listed in Table 5, which demonstrates as follows:

(a) profiles showing instrumental broadening only are well expressed by Modified Lorentzian function.

(b) profiles from specimens showing large strain broadening and little size broadening are also well expressed by Modified Lorentzian function.

(c) profiles from a specimen showing large size broadening and little strain broadening are well expressed by Lorentzian function.

(d) the values of an integral breadth calculated with three types of presumptive functions are well consistent with each other.

These are consistent with the conclusions that:

(1) both instrumental broadening and strain broadening are assumed to be Modified Lorentzian function and size broadening to Lorentzian function.

(2) Modified Lorentzian function can be adopted as a calculated profile shape function for the profile fitting procedure to obtain an integral breadth.

Appendix 2. Brief explanation of samples

(1) Quartz phenocrysts in Cretaceous welded tuff, originally crystallized as high quartz, at the Ikuno mine, Hyogo Prefecture whose diameters are some 1 or 2 mm (IK 01).

(2) Bedded chert metamorphosed by the Ryoke regional metamorphism to the north of Kasagi, Kyoto Prefecture (KA 01–05). Most of them are characterized by equant and polygonal grains whose mean diameters vary from some 5 μm to some 100 μm. A texture suggestive of secondary recrystallization is partly recognized in the samples of large grain sizes (KA 04–05). As for KA 10b, special treatments were applied in order to obtain very fine powders with little microstrain. After the grindation for an hour, powders whose diameters are less than 1 μm were obtained by means of precipitation using the Stokes' formula.

(3) Bedded chert in the contact aureola, to the east of the Otani mine, Kyoto Prefecture (OT 01–05). All of them are characterized by equant and polygonal grains whose mean diameters vary from some 0.5 μm to some 30 μm.

(4) Chert in the greenstone body at Onogahara, Ehime Prefecture, which is characterized by equant and polygonal grains whose mean diameter is some 10 μm (ON 01). It is considered to be subjected to the Sanbagawa regional metamorphism.

(5) Hardly metamorphosed Triassic bedded chert in Unuma, Gifu Prefecture, nearly the same localities of Fig. 1 in SHIBATA and MIZUTANI (1982) (UN 01–02).

(6) Length-fast chalcedony (AG 01–03) and macrocrystalline quartz (AG 04) in Brazilian zoned agate. It was devided into four speimcens from the rim to the core. The photomicrographs are shown in Plate.

References

VAN ARKEL, A.E. (1925): Over de Deformatie van het Kristalrooster van metalen door Mechanische Bewerking. *Physica,* **5**, p. 208–212.

BURSILL, L.A. and MCLAREN, A.C. (1965): Transmission electron microscope observations of fracture in quartz and zircon. *Jour. Appl. Phys.*, **36**, p. 2084–2085.

FLÖRKE, O.W., KÖHLER-HERBERTZ, B., LANGER, K. and TONGES, I. (1982): Water in microcrystalline quartz of volcanic origin: agates. *Contrib. Mineral. Petrol.*, **80**, p. 324–333.

GROSS, K.A. (1965): X-ray line broadening and stored energy in deformed and annealed calcite. *Phil. Mag.*, **12**, p. 801–813.

GROSS, K.A. and PATERSON, M.S. (1965): Natural X-ray line broadening in limestones and marbles. *Am. Jour. Sci.*, **263**, p. 238–244.

GUINIER, A. (1956): *Théorie et Technique de la Radiocristallographie.* Paris, Dunod. (cited to a Japanese translation by KOURA, K. *et al.* (1963), Rigaku Denki Pub.)

HANSS, R.E., MONTAGUE, B.R., DAVIS, M.K., GALINDO, C. and HORZ, F. (1978): X-ray diffractometer studies of shocked materials. *Proc. Lunar. Planet. Sci. Conf. 9th*, p. 2773–2787.

HATHAWAY, J.C. (1972): X-ray mineralogy studies—Leg. 11, pt. 2. In HOLLISTER, C.D., EWING, J.I. *et al.*, 1972, *Initial Reports Deep Sea Drilling Project*, **11**, U.S. Govt. Printing Office, Washington, D.C., p. 772–789.

HÖRTZ, F. and QUAIDE, W.L. (1973): Debye-Scherrer investigations of experimentally shocked silicates. *Moon*, **6**, p. 45–82.

JONES, F.W. (1938): The measurement of particle size by the X-ray method. *Proc. Roy. Soc.* A, **166**, p. 16–43.

DE KEIJSER, TH, H. and MITTEMEIJER, E.J. (1977): Correction for erorrs in microstrain values from X-ray diffraction line profiles. *Phil. Mag.*, **36**, p. 1261–1264.

KLUG, H.P. and ALEXANDER, L.E. (1954): *X-ray diffraction procedures for ploycrystalline and amorphous materials.* John Wiley and Sons, New York.

MIEVE, G., GRAETSCH, H. and FLÖRKE, O.W. (1984): Crystal structure and growth fabric of length-fast chalcedony. *Phys. Chem. Minerals*, **10**, p. 197–199.

MURATA, K.J. and NORMAN, II, M.B. (1976): An index of crystallinity for quartz. *Am. Jour. Sci.*, **276**, p. 1120–1130.

NAGAO, H. and AIKAWA, N. (1983): Differential stress of low P/T type Ryoke regional metamorphism, in central Kinki, Japan. *Jour. Japan. Assoc. Min. Pet. Econ. Geol.*, **78**, p. 363–375.

PATERSON, M.S. (1959): X-ray line broadening in plastically deformed calcite. *Phil. Mag.*, **4**, p. 451–466.

ROSENTHAL, D. and KAUFMAN, M. (1952): X-ray line broadening of plastically deformed marble. *Jour. Appl. Phys.*, **23**, p. 600–601.

SCHNEIDER, H., VASUDEVAN, R. and HORNEMANN, U. (1984): Deformation of experimentally shock-loaded powders: X-ray line broadening studies. *Phys. Chem. Minerals*, **10**, p. 142–147.

SCHÖENING, F.R.L. (1965): Strain and particle size values from X-ray line breadths. *Acta Cryst.*, **18**, p. 975–976.

SCHÖENING, F.R.L., *AN NIEKERK, J.N. and HAUL, R.A.W. (1952): Influence of the apparatus function on crystallite size determination with Geiger counter spectrometers. *Proc. Phys. Soc.*, B, **65**, p. 528–535.

SHIBATA, K. and MIZUTANI, S. (1982): Isotopic ages of Jurassic siliceous shale and Triassic bedded chert in Unuma, Central Japan. *Geochem. Jour.*, **16**, p. 213–223.

STOKES, A.R. (1948): A numerical Fourier-analysis method for the correction of widths and shapes of line on X-ray powder photographs. *Proc. Phys. Soc. London* NB, **61**, p. 382–391.

TAYLOR, A. (1961): *X-ray metallography.* John Wiley and Sons, New York.

WARREN, B.E. (1941): X-ray diffraction methods. *Jour. Appl. Phys.*, **12**, p. 375–383.

WARREN, B.E. (1959): X-ray studies of deformed metals. In CHALMERS, B. and KING, R. (eds.) *Progress in Metal Physics*, **8**, p. 147–202.

WARREN, B.E. and AVERBACV, B.L. (1950): The effect of cold-work distortion on X-ray patterns. *Jour. Appl. Phys.*, **21**, p. 595–599.

WARREN, B.E. and AVERBACH, B.L. (1952): The separation of cold-work distoriton and particle size broadening in X-ray patterns. *Jour. Appl. Phys.*, **23**, p. 497–498.

WOOD, W.A. and RACHINGER, W.A. (1949): Crystallite theory of strength of metals. *Jour. Inst. Metal*, **75**, p. 571–594.

YOUNG, R.A., GERDES, R.J. and WILSON, A.J.C. (1967): Propagation of some systematic errors in X-ray line profile analysis. *Acta Cryst.*, **22**, p. 155–162.

YOUNG, R.A. and WILES, D.B. (1982): Profile shape functions in Rietveld refinements. *Jour. Appl. Cryst.*, **15**, p. 430–438.

Explanation of plate

Photomicrographs of studied specimens.

Fig. 1 Cross section of the zoned agate. Bar represents 1 cm in length.

Fig. 2–3 Parts of zoned agate. (2): AG 02, (3): AG 03. Bar represents 200 μm in length.

Fig. 4–5 Metachert of the contact aureola. (4): OT 01, (5) OT 05. Bar represents 100 μm in length.

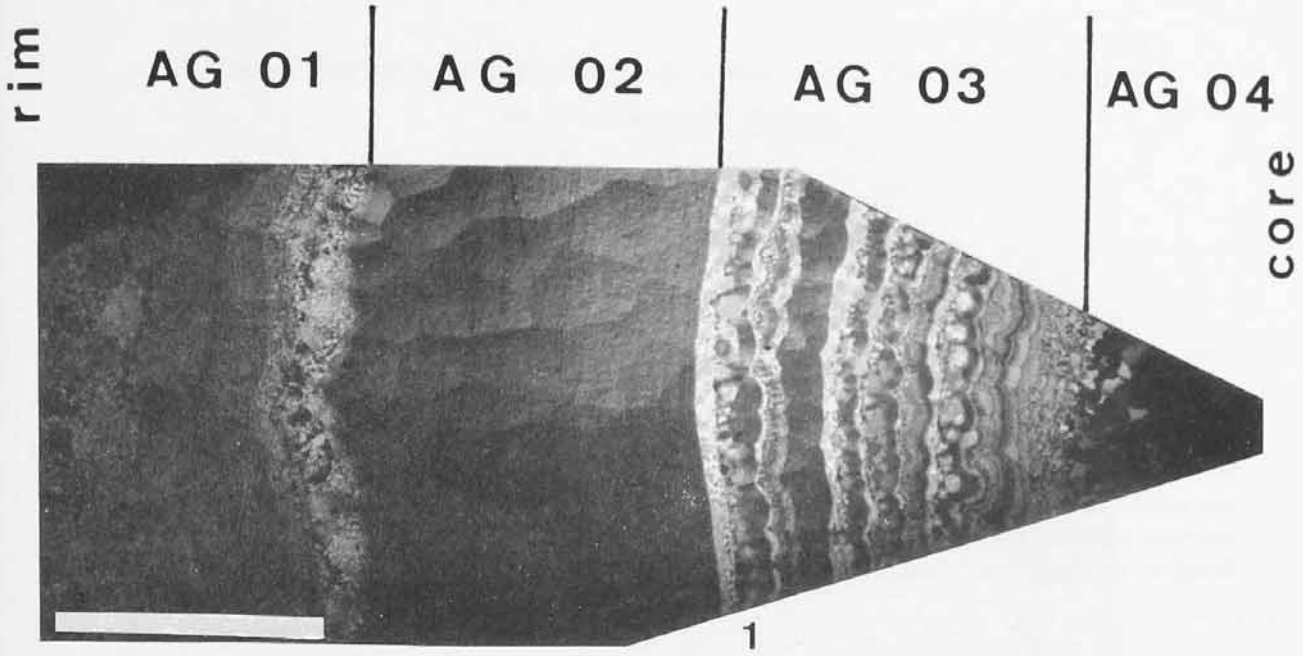

1

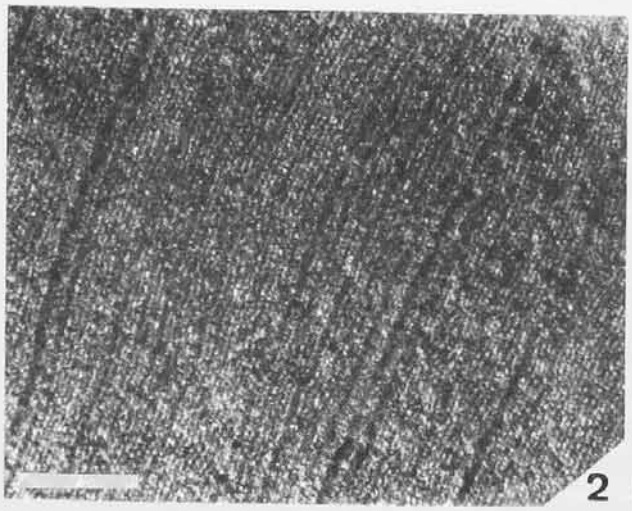

2

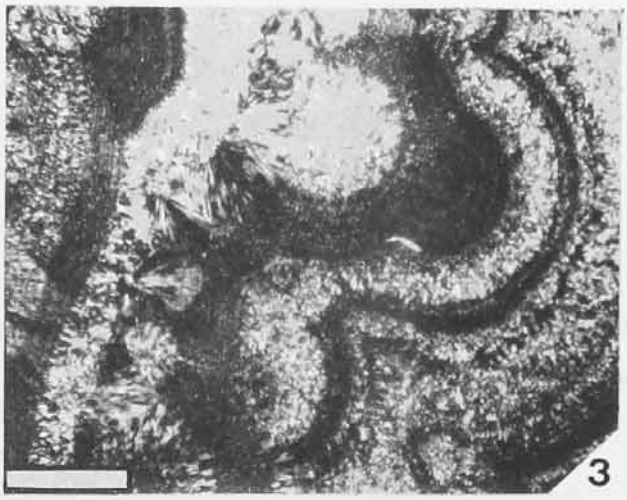

3

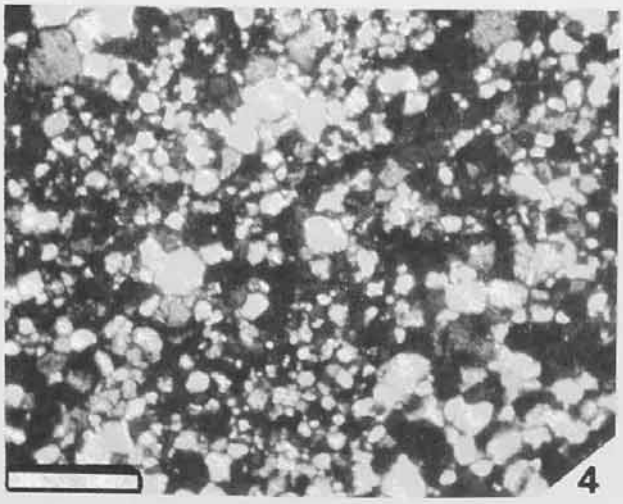

4

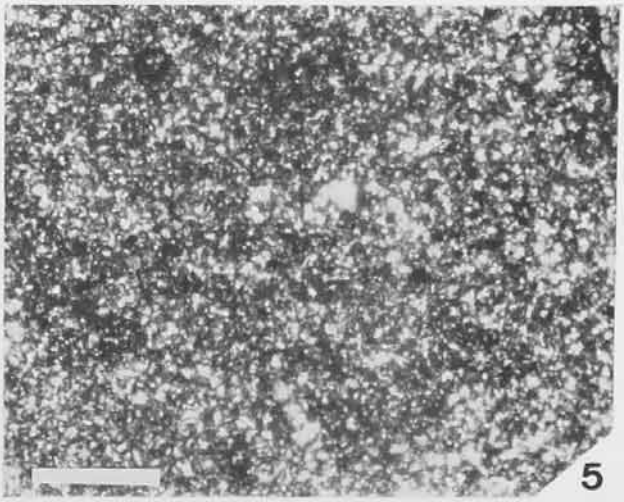

5